

## Local HI emissivity and implications for cosmic-ray spectra

JEAN-MARC CASANDJIAN<sup>1</sup> ON BEHALF OF THE FERMI-LAT COLLABORATION

<sup>1</sup> SAP-IRFU, CEA Saclay

casandjian@cea.fr

**Abstract:** Cosmic-ray electrons and nuclei interact with the Galactic interstellar gas and produce high-energy gamma rays. The production processes are mainly Bremsstrahlung and hadronic interactions. Their emission rate, called emissivity, provide a unique indirect probe of the cosmic-ray flux. We present a precise measure of the HI emissivity in the solar neighborhood performed by Fermi and show it can be used to derive constraints on the interstellar cosmic-ray proton and alpha spectra. We provide an experimental evidence of cosmic-ray solar modulation and test the force-field approximation for protons and heliums above 1 GeV/nucleon.

**Keywords:** interstellar gas, cosmic-ray,  $\gamma$ -ray, Fermi

### 1 Introduction

The theory behind cosmic rays (CR) and interstellar medium (ISM) interaction initiated in the fifties was confronted with early balloons and flight experiments in the sixties. In the eighties, [20] extracted the H I emissivity in three energy bands from Cos-B data, which was later improved by [25] with a more robust interstellar emission modeling. Using EGRET, [26] extracted the first precise spectrum of H I  $\gamma$ -ray emissivity. The Large Area Telescope (LAT) is the main  $\gamma$ -ray detector of the *Fermi Gamma-ray Space Telescope* (*Fermi*) satellite, it collects  $\gamma$ -ray in the energy range from 20 MeV to more than 300 GeV. [1] used LAT photons in a mid-latitude region in the third quadrant deprived of known molecular clouds to extract the H I emissivity in 13 logarithmically sliced energy bins from 100 MeV to 9.05 GeV. They masked the bright sources, and correlated for each energy bin the H I column density,  $N(\text{H I})$ , to the LAT counts with inverse-Compton subtracted.

Here we have extended the work of [1] to the whole longitude range and to latitude from  $10^\circ$  to  $70^\circ$  and  $-70^\circ$  to  $-10^\circ$  to derive from 4 years of LAT data the local H I emissivity from the simple and robust template method.

We then compared those emissivities with the ones computed from heliospheric CR observations and  $\gamma$ -ray production cross-sections.

### 2 Data Selection

We used 4 years of data recorded from August 2008 to August 2012. We excluded from this time interval the periods where intense transients occurred. That resulted in 55 million LAT counts that we binned into 28 energies logarithmically spaced from 50 MeV to 50 GeV. The highest 4 energy bins were added-up two by two to increase the statistics and fit stability. We used events derived from Pass 7\_V15 and the corresponding set of instrument response function. We used the Clean selection that has a reduced instrumental background compared to the Source selection<sup>1</sup>. To lower the number of  $\gamma$ -rays originating from the interaction between CR protons and the earth limb, we removed from our selection all photons with a zenith angles larger than  $100^\circ$ . Remaining limb photons were modeled and subtracted from the data.

### 3 ISM gas census

Most LAT photons come from CR protons impinging on atomic and molecular hydrogen and, to a less extent for the energies considered here, electrons deflected by hydrogen nuclei. We used the all-sky Leiden-Argentina-Bonn (LAB) [17] composite survey to obtain the atomic hydrogen  $N(\text{H I})$  column densities with the assumption of a uniform spin temperature ( $T_S$ ). We used CO as a surrogate tracer for molecular hydrogen. The velocity integrated CO intensities  $W(\text{CO})$  were obtained from the Center for Astrophysics compilation [7] as well as new dedicated observations obtained at mid-latitudes, up to  $|b| = 30^\circ$  in the northern hemisphere, with the same telescope. In our study, we did not assume any value for the  $\text{H}_2$ -to-CO conversion factor; on the contrary, we obtained it from the fit. The dark gas [14] not traced by radio emission was accounted for by a template extracted from the residuals of reddening E(B-V) map [23] after removing the structures correlated with  $N(\text{H I})$  and  $W(\text{CO})$ . The ionized hydrogen H II was estimated from pulsar dispersion measures and modeled by NE2001 [6]. To allow for a Galactocentric gradient of CR flux in the Galaxy, the  $N(\text{H I})$ ,  $N(\text{H II})$  column-densities and  $W(\text{CO})$  intensities have been derived for several Galactocentric rings. This work interprets the emissivities of the local ring corresponding to Galactocentric distances from about 8 to 9.5 kpc.

### 4 Fitting Procedure

The template method has been widely used since the beginning of diffuse  $\gamma$ -ray astronomy [19, 25, 9, 14, 2]. The fitting procedure is similar to the one used to build the *Fermi* interstellar emission model. We modeled the  $\gamma$ -ray intensity as a linear combination of gas tracers, Galactic inverse-Compton (IC), extragalactic background intensity, large structures (LS) and point sources (eq. 1). The large structures include both the *Fermi* bubbles and Loop I emission. Loop I template was obtained from the 408 MHz synchrotron survey. The *Fermi* bubbles shapes and intensity were deduced iteratively. We convolved the modeled intensity in each energy bin with the point spread function (PSF) and deduced gas emissivities, inverse-Compton normalization and isotropic emission from a maximum-likelihood fit. We

1. <http://fermi.gsfc.nasa.gov/ssc/>.

have used a binned maximum-likelihood method with Poisson statistics using maps binned in HEALPix<sup>2</sup> [12] with a  $N_{\text{side}}$  of 256 so the bin size is approximately  $0.25 \times 0.25$  degree. We used the Science Tool<sup>1</sup> *gtrspgen* to correct for the LAT energy dispersion.

$$\begin{aligned}
 N_{\text{pred}}(l, b) = & \int \int d\Omega_k \left( \sum_{i=\text{rings}} [q_{HI,i} N_{HI}(r_i, l_k, b_k) \right. \\
 & + q_{CO,i} W_{CO}(r_i, l_k, b_k) + q_{HII,i} N_{HII}(r_i, l_k, b_k)] \\
 & + q_{DG} I_{DG}(l_k, b_k) + q_{IC} I_{IC}(l_k, b_k) \\
 & + q_{LS} I_{LS}(l_k, b_k) + I_{iso} \left. \right) \varepsilon(l_k, b_k) PSF(l, b, l_k, b_k) \\
 & + \sum_{j=\text{sources}} F_j \varepsilon(l_j, b_j) PSF(l, b, l_j, b_j)
 \end{aligned}$$

#### 4.1 Point and Extended Sources

We fitted 2179 point sources listed in a preliminary version of the 3FGL catalog [5]. We modeled each source with the Science Tool *gtrsrcmaps* that convolves through the instrument response at each source position and in each energy bin. We verified that the fluxes obtained here are compatible with the 2FGL catalog for most sources with low variability index. We also included in the fit the  $\gamma$ -ray emission from the sun, the moon and the following extended sources: Centaurus A, Cygnus Loop, HESSJ1614-518, HESSJ1616-508, HESSJ1632-478, HESSJ1825-137, HESSJ1837-069, IC443, LMC, MSH15-52, PuppisA, RXJ1713.7-3946, S147, SMC, Vela Junior, VelaX, W28, W30, W44, W51C and gamma Cygni.

### 5 Systematic Errors

We investigated three major sources of systematic errors: the H I spin temperature ( $T_S$ ), the modeling of the Galactic inverse Compton and the systematic error in LAT effective area.

When deriving  $N(\text{H I})$  from radio survey we need to correct for the 21 cm H I line opacity that depends on its  $T_S$ . Since CR interact with H I independently of its  $T_S$  and since the Galaxy is optically thin to  $\gamma$ -ray at energies considered here, we can compare the LAT counts map with models based on  $N(\text{H I})$  derived with various  $T_S$ . The optical thickness of local H I does not make it sensitive enough to variation of  $T_S$ , we used the outer Galaxy ( $90^\circ \leq l \leq 270^\circ$ ) to obtain the H I  $T_S$  that gives the best fit to the data. We did not use the inner Galaxy that has too many excesses or deficit compared to the model likely not related to  $T_S$ . We investigated seven  $T_S$  from 90 K to 400 K. For each temperature, we derived a H I column density and a dark gas map. We used those maps in a fit of the outer Galaxy.  $T=140$  K gives a model that fits the best the LAT counts. We used the values 125 K and 170 K to estimate the uncertainty in the emissivity related to the  $T_S$ . Those values are much farther apart from the ones given by the likelihood, it corresponds to values where a noticeable discrepancy is observed through the fit residual map. Note that we assumed here an uniform  $T_S$  and corrected this approximation by fitting both the positive and negative residuals of the dark gas map. The  $T_S$  of 140 K is therefore the temperature that best fit the outer Galaxy under the assumption that the dust column density

of [23] is accurate and that the dust is mixed with all the phases of H I.

As shown in [3] there is not a unique set of Galprop<sup>4</sup> [27] propagation parameters that can model the *Fermi* sky. Since we rely on Galprop for the morphology of the inverse-Compton  $I_{IC}$  map, we investigated the effect of three sets of Galprop parameters called 54\_z10G4c5rS, 54\_77Xvarh7S and LRYusifovXCO4z6R30\_Ts150\_mag2. It corresponds to diffusive reacceleration models with different source distributions, halo size and electrons source spectrum. The variation induced by the use of various models is low since the spatial structures of  $N(\text{H I})$  allow a good separation from the smooth IC map. We used the most recent inverse Compton map obtained with the version LRYusifovXCO4z6R30\_Ts150\_mag2 for the final  $\gamma$ -ray fit and added in the systematic errors the variation obtained from the other IC templates.

Finally we used the recommended Pass 7\_V15 systematic error<sup>2</sup> for the LAT effective area: 20% at 50 MeV, 10% at 100 MeV, 5% at 560 MeV, 10% at 10 GeV and we extrapolated linearly those values. This uncertainty largely dominates the others in the whole energy range.

We also verified that the potential incorrect modeling of the Galactic plane and the modeling of the large structures has no effect on the emissivities by using several latitude cuts and regions away from Loop I.

## 6 Results

We fitted to the LAT counts the model given by Eq. 1. The upper map of Fig. 1 shows the total *Fermi* 4 years accumulated number of counts above 360 MeV. In the same figure, below, the point and extended sources as well as the isotropic emission were subtracted leading to an accumulated counts map associated only with the interstellar emission. Close dense molecular clouds like Orion or Taurus are visible in this map. We can also see at high latitude the more diffuse structure of counts resulting from the interaction of CR with H I. We extracted those counts associated with H I by removing from the LAT  $\gamma$ -ray map all the templates and sources of Eq. 1 except the ones associated with  $N(\text{H I})$ . Fig. 2 shows the correlation obtained between this  $\gamma$ -ray intensity associated with H I and the predicted intensity derived from  $N(\text{H I})$ .

For each of the 26 energy bands we derived from likelihood minimization the integrated emissivity  $q_{HI}$  that were transformed into differential emissivity. The emissivity corresponding to the local ring, given here per H I atom, is plotted in Fig. 3 at energies corresponding the logarithmic mid-point of the band.

## 7 Interpretation

### 7.1 Production cross-section

Most  $\gamma$ -ray with energies between 100 MeV and 50 GeV originate from the decay of  $\pi^0$  produced in hadronic collisions when CR protons with energies from 0.5 to  $10^3$  GeV interact with ISM nuclei. At those energies, the vast majority of  $\pi^0$  are produced with a low transverse momentum transfer through soft interactions where the large strong force coupling constant prevents the use of a perturbative

2. <http://healpix.jpl.nasa.gov>

4. <http://galprop.stanford.edu>

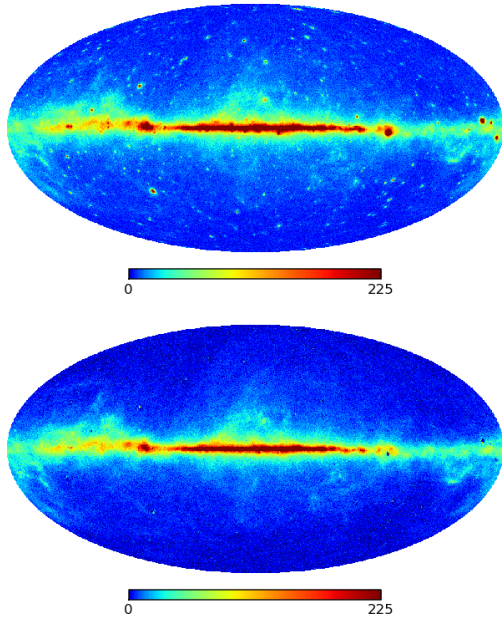


**Figure 1:** Total LAT counts per pixels above 360 MeV (above) in sqrt color scaling with a pixel size of  $0.25^\circ$ . When point and extended sources and the isotropic emission are subtracted, we obtain the counts correlated with the interstellar emission (below).

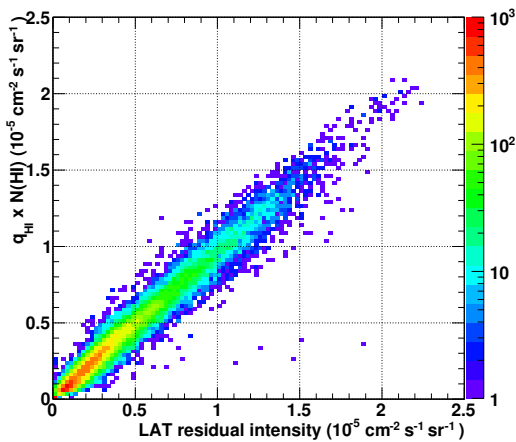


**Figure 2:** LAT residual intensity correlated with atomic hydrogen column density for latitude of  $10\text{deg}-70\text{deg}$

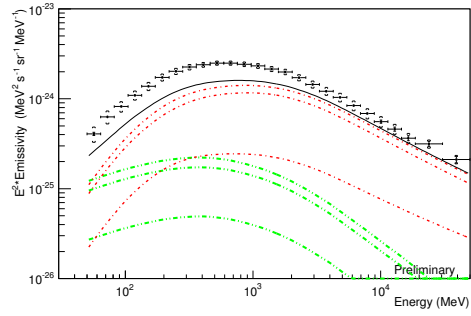


**Figure 3:** Differential local HI emissivity versus  $\gamma$ -ray energy. The vertical error bars correspond to statistical uncertainties while systematics are represented by square brackets, the horizontal bars correspond to the bins energy width. The measured emissivities are compared to calculated ones from heliospheric CR observations with no solar demodulation. The green curve represents the  $\gamma$ -ray from electrons Bremsstrahlung on helium nuclei (lower) and atomic hydrogen nuclei (middle). The red curves indicates the production of  $\gamma$ -ray from hadronic collisions between the ISM and helium (lower) and protons plus nuclei heavier than helium (middle). Their sums are also shown (upper)

QCD approach. This regime is poorly understood and the  $\pi^0$  cross section is obtained mainly through phenomenological models. In this work we used the  $\gamma$ -ray production cross-section of [18], [15] and [24]. The contribution from  $\eta$  that appears to be overestimated by [15] was reduced by a factor 8 to match the experimental cross-section measured in [4]. An alternative approach, using an updated version of [16] is presented in [8].

Fermi detects  $\gamma$ -ray resulting not only from the interaction of p-p but also from the interaction of CR with ISM nuclei. We used [22] to scale  $\sigma_{pp}$  to nucleus-nucleus cross-section. Table 1 lists the scaling factor for collision induced by proton and helium CR after including an ISM relative abundance of [21, 22]. CR heavier than helium colliding with the ISM also contribute to the total  $\gamma$ -ray yield. Their relative abundances were estimated from Table 1 of [10]. Using those abundances we obtained a correction equivalent to  $0.116\sigma_{pp}$  that we added to  $\sigma_{p,ISM}$  so that  $\sigma_{p+heavy,ISM} = 1.503\sigma_{pp}$ . For the Bremsstrahlung of CR electrons of about 0.1 to 50 GeV we used the formula of [13].

**Table 1:** Factors used to scale  $\sigma_{pp}$

Proj	Target					
	H	He	CNO	Mg-Si	Fe	sum
H	1.	0.366	0.016	0.004	0.001	1.387
He	3.68	1.363	0.058	0.015	0.005	5.12

## 7.2 Local interstellar spectra

To calculate the HI emissivities and compare them to the ones measured by *Fermi*, we must fold the  $\gamma$ -ray production

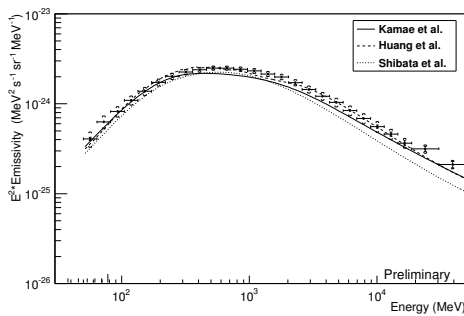


**Figure 4:** Differential local H I emissivity compared to prediction based on [18] (solid), [15] (dashed), and [24] (dotted). In this example the CR flux was demodulated with the potential  $\Phi = 400MV$

cross-sections with proton, helium and electron LIS. We used the proton and alpha spectra measured by Pamela and Atic. At low energy it is extrapolated guided by the two lowest energy points of AMS. The flux is solar-demodulated by the simple force-field approximation [11].

The electrons that produce  $\gamma$ -ray at energies considered here also spiral around the Galactic magnetic field lines and produce radio synchrotron with frequencies from a few MHz to approximately ten GHz. This range corresponds to the one [28] used to derive an electron LIS. We fixed our electron spectrum (and so the Bremsstrahlung contribution) to the flux calculated by [28].

### 7.3 Comparison with experiment

The predicted emissivities calculated with Kamae cross-section are compared to the ones extracted from *Fermi* in Fig. 3. In this figure we did not demodulate the proton nor helium spectra. We observe a disagreement between the calculated and the measured emissivities. In figure 4 we compared our results with predicted emissivities using various production cross-section calculated with a solar modulation potential of  $\Phi = 400MV$ . We obtain a good agreement and observe variation of the order of 20% between the various models. The value of modulation potential  $\Phi$  is given here as an illustration, it does not result from a fit.

## 8 Conclusion

We derived the H I local  $\gamma$ -ray emissivity from 4 years of *Fermi* survey. Its spectrum was measured with precision and systematic uncertainties were evaluated. We compared them with predicted ones using various production cross-section and heliospheric proton and alpha fluxes. We obtain a good agreement when those CR fluxes are solar-demodulated. The accuracy of  $\gamma$ -ray production cross-sections will limit the precision of CR spectra that can be inferred from this study.

The *Fermi* LAT Collaboration acknowledges support from a number of agencies and institutes for both development and the operation of the LAT as well as scientific data analysis. These include NASA and DOE in the United States, CEA/Irfu and IN2P3/CNRS in France, ASI and INFN in Italy, MEXT, KEK, and JAXA in Japan, and the K. A. Wallenberg Foundation, the Swedish Research Coun-

cil and the National Space Board in Sweden. Additional support from INAF in Italy and CNES in France for science analysis during the operations phase is also gratefully acknowledged.

## References

- [1] Abdo, A. A. et al. 2009, *The Astrophysical Journal*, 703, 1249
- [2] Abdo, A. A. et al. 2010, *The Astrophysical Journal*, 710, 133
- [3] Ackermann, M. et al. 2012, *The Astrophysical Journal*, 750, 3
- [4] Aguilar Benitez, M. et al 1991 *Zeitschrift fr Physik C Particles and Fields*, 50, 405
- [5] Ballet, J. et al. 2013, 33th International Cosmic Ray Conference, id 1153
- [6] Cordes, J. M., & Lazio, T. J. W. 2002, eprint arXiv, 7156
- [7] Dame, T. M., Hartmann, D., & Thaddeus, P. 2001, *The Astrophysical Journal*, 547, 792
- [8] Dermer, C.D. et al. 2013, 33th International Cosmic Ray Conference, id 1165
- [9] Digel, S. W., Aprile, E., Hunter, S. D., Mukherjee, R., & Xu, F. 1999, *The Astrophysical Journal*, 520, 196
- [10] Gaisser, T. K. et al. 2001, 27th International Cosmic Ray Conference, 5, 1643
- [11] Gleeson, L. J., & Axford, W. I. 1968, *Astrophysical Journal*, 154, 1011
- [12] Górski, K. M., Hivon, E., Banday, A. J., Wandelt, B. D., Hansen, F. K., Reinecke, M., & Bartelmann, M. 2005, *The Astrophysical Journal*, 622, 759
- [13] Gould, R. J. 1969, *Physical Review*, 185, 72
- [14] Grenier, I. A., Casandjian, J.-M., & Terrier, R. 2005, *Science*, 307, 1292
- [15] Huang, C.-Y., Park, S.-E., Pohl, M., & Daniels, C. D. 2007, *Astroparticle Physics*, 27, 429
- [16] Kachelrieß, M., & Ostapchenko, S. 2012, *Physical Review D*, 86, 43004
- [17] Kalberla, P. M. W., Burton, W. B., Hartmann, D., Arnal, E. M., Bajaja, E., Morras, R., & Pöppel, W. G. L. 2005, *Astronomy and Astrophysics*, 440, 775
- [18] Kamae, T., Karlsson, N., Mizuno, T., Abe, T., & Koi, T. 2006, *The Astrophysical Journal*, 647, 692
- [19] Lebrun, F., & Paul, J. A. 1979, 16th International Cosmic Ray Conference, 12, 13
- [20] Lebrun, F. et al. 1982, *Astronomy and Astrophysics*, 107, 390
- [21] Meyer, J.-P. 1985, *Astrophysical Journal Supplement Series*, 57, 173
- [22] Mori, M. 2009, *Astroparticle Physics*, 31, 341
- [23] Schlegel, D. J., Finkbeiner, D. P., & Davis, M. 1998, *Astrophysical Journal* v.500, 500, 525
- [24] Shibata, T. et al. 2013, eprint arXiv, 1304.0879S
- [25] Strong, A. W. et al. 1988, *Astronomy and Astrophysics*, 207, 1
- [26] Strong, A. W., & Mattox, J. R. 1996, *Astronomy and Astrophysics*, 308, L21
- [27] Strong, A. W., Moskalenko, I. V., & Ptuskin, V. S. 2007, *Annual Review of Nuclear and Particle Systems*, 57, 285
- [28] Webber, W. R., & Higbie, P. R. 2008, *Journal of Geophysical Research*, 113, 11106